



## Article

# Development of AgFeO<sub>2</sub>/rGO/TiO<sub>2</sub> Ternary Composite Photocatalysts for Enhanced Photocatalytic Dye Decolorization

Nasir Shehzad <sup>1,†</sup>, Muhammad Zafar <sup>2,†</sup>, Muhammad Ashfaq <sup>3,†</sup>, Abdul Razzaq <sup>1,†</sup>, Parveen Akhter <sup>3</sup>, Nabeel Ahmad <sup>1</sup>, Ainy Hafeez <sup>1</sup>, Kshaf Azam <sup>1</sup>, Murid Hussain <sup>1,\*</sup>  and Woo Young Kim <sup>4,\*</sup> 

- <sup>1</sup> Department of Chemical Engineering, COMSATS University Islamabad, Lahore 54000, Pakistan; nasir.shehzad@cuilahore.edu.pk (N.S.); abdulrazzaq@cuilahore.edu.pk (A.R.); nabeelahmad@cuilahore.edu.pk (N.A.); ainyhafeez@cuilahore.edu.pk (A.H.); kshaf@hotmail.co.uk (K.A.)
- <sup>2</sup> Institute of Energy and Environmental Engineering, University of the Punjab, Lahore 54590, Pakistan; zafar.ieee@pu.edu.pk
- <sup>3</sup> Department of Chemistry, The University of Lahore, 1-Km Raiwind Road, Lahore 54000, Pakistan; ashfaqishaq2@gmail.com (M.A.); parveen.akhter@chem.uol.edu.pk (P.A.)
- <sup>4</sup> Department of Electronic Engineering, Faculty of Applied Energy System, Jeju National University, Jeju Special Self-Governing Province, Jeju-si 63243, Korea
- \* Correspondence: drmhussain@cuilahore.edu.pk (M.H.); semigumi@jejunu.ac.kr (W.Y.K.)
- † These authors contributed equally to this work.

Received: 11 August 2020; Accepted: 9 October 2020; Published: 12 October 2020



**Abstract:** Dyestuff is one of the most widely released pollutants into the environment. Many approaches have been considered to deal with the dye removal from polluted water such as adsorption, ultrafiltration, osmosis, solvent extraction and photocatalytic degradation. The photocatalytic degradation process is one of the most beneficial, economical and environmentally friendly ways to degrade the organic pollutants from wastewater. In this study, an efficient ferrite-based photocatalyst, AgFeO<sub>2</sub>/rGO/TiO<sub>2</sub> was successfully developed using simple deposition and reflux method. Physical, chemical and structural properties were analyzed by using XRD, FTIR Raman and PL spectroscopy. The efficiency of photocatalyst was investigated for the decolorization of methyl blue (MB) dye and activity was measured through UV-vis spectroscopy. The effect of parameters like pH, concentrations of MB dye, and loading of silver ferrite (AgFeO<sub>2</sub>) was investigated. The study depicted that the properties of TiO<sub>2</sub> were improved due to addition of silver ferrite and reduced graphene oxide (rGO). The 2.5% AgFeO<sub>2</sub>/rGO/TiO<sub>2</sub> exhibited the highest efficiency and completely degraded the 50 ppm of MB dye in 30 min. The parametric study revealed that dye decolorization is faster in a neutral solution than in basic and acidic medium. The higher performance of the photocatalyst was attributed to the reduced charge recombination and improved optical properties. Thus, AgFeO<sub>2</sub>/rGO/TiO<sub>2</sub> can be a potential composite for photocatalytic dye degradation and other photocatalytic applications under UV-Visible light irradiations.

**Keywords:** ternary composite; photocatalysis; methyl blue dye degradation; wastewater treatment

## 1. Introduction

Water pollution is one of the biggest threats to the ecological system. Around 80% of the wastewater produced in the world is discharged into environment without proper treatment, polluting freshwater resources [1]. The industrial sector is one of the largest sources of water pollution, which releases toxic chemicals into local water bodies. Industrial wastewater treatment gets the least attention, particularly

in developing countries, due to which around 70% of effluents go untreated [2]. Dyestuffs from textile and food industry are considered to be one of the crucial water pollutants. Dyes are complex organic compounds which are non-biodegradable in nature and have adverse health effects such as cancer, asthma, skin allergies, and respiratory diseases [3].

Many approaches have been considered to deal with the dye removal from polluted wastewater such as adsorption, microbiological decomposition, enzymatic decomposition, ultrafiltration, osmosis, microfiltration, and photocatalytic dyes degradation [4]. Adsorption is expensive when considering the large quantity of adsorbent to be used, recovery and regeneration cost of adsorbent. Microbial and enzymatic decomposition take place under particular conditions and controlled environment which limit the application at very large industrial scale. Ultrafiltration and osmosis process have limitations due to membrane fouling, higher process costs and operational problems. [5]. Photocatalytic dye degradation is considered to be one of the most beneficial and energy efficient technique since it uses direct solar light irradiations without producing any hazardous side products [6].  $\text{TiO}_2$  has been widely used for photocatalytic applications including decomposition of toxic dyestuffs from wastewater. However, the large bandgap (3.2 eV) and high recombination reaction rates of photogenerated electron–hole pairs limits its photocatalytic efficiency [5,7]. Moreover, due to the wide band gap, the photocatalytic reactions of  $\text{TiO}_2$  can only be carried out in UV or near UV irradiation, which occupies only <4% of the sunlight spectrum on earth [5,7]. Recently, research is being focused on developing photocatalysts with narrow band gap that could work in visible light to fully utilize solar light potential [8]. Therefore, heterogeneous photocatalysis has been studied widely for the photocatalytic degradation of dyes.

The electron–hole recombination and wide bandgap of the  $\text{TiO}_2$  can be reduced by using different modifications processes such as coupling with semiconductors, and surface photosensitization [3–5]. Graphene supported  $\text{TiO}_2$  composites have recently shown higher performance owing to the high mobility of electrons resulting in low charge recombination [9]. The large surface area of graphene  $2600 \text{ m}^2/\text{g}$  creates much attraction towards itself [10]. The thermal conductivity ( $\sim 3000 \text{ Wm}^{-1}\text{K}^{-1}$ ) and mechanical strength of  $\text{TiO}_2$  (1060 GPa) are reported [11]. The modification of  $\text{TiO}_2$  with rGO is an attractive route for wastewater treatment in the visible region [12,13]. Integration of the  $\text{TiO}_2$  with reduced graphene oxide (rGO) not only increase the visible light absorption capability but also decrease electric charge recombination. In addition, rGO- $\text{TiO}_2$  have high surface area and have higher adsorption rate which enhance the performance of photocatalytic dyes degradation [14]. Doping with carbon derivatives leads to formation of Ti–O–C bonds which enables the absorption of light into visible light region [15]. Similarly, introducing metal as the dopant into the crystal lattice of  $\text{TiO}_2$  catches the electrons and holes temporarily to reduce the electron–hole recombination and enhance the photocatalytic activity [13,14].

Many researchers have investigated the rGO- $\text{TiO}_2$  composites to eliminate and degrade the pollutants from water such as methyl orange, methylene blue, methyl blue (MB) diphenhydramine and rhodamine B [12,15–17]. By using solvothermal process, Lui et al. [14] prepared graphene-wrapped hierarchical  $\text{TiO}_2$  nanoflowers. Under UV-visible irradiation, hierarchical  $\text{TiO}_2$  nanoflowers showed excellent performance for the degradation of methylene blue. Owing to the high conductivity of rGO, it decreases the recombination of electron–hole pairs, and consequently increases the degradation rate [18]. Muthirulan et al. [18] prepared rGO/ $\text{TiO}_2$  nanocomposite reported graphene played the role of electron acceptor and effectively reduced the electron–hole recombination and enhance the photocatalytic degradation of acid orange 7 dye. Photocatalytic efficiency of rGO/ $\text{TiO}_2$  is still far from practical consideration compared to adsorption and ultrafiltration methods.

There is an increasing trend to tailor the multinary rGO/ $\text{TiO}_2$  composites with improved photocatalytic performance for several of photocatalytic application including  $\text{CO}_2$  reduction, water splitting and dyes degradation [19–21]. Samsudin et al. [21] integrated the  $\text{TiO}_2$  and  $\text{BiVO}_4$  through the wet impregnation method. The rGO/ $\text{TiO}_2$ / $\text{BiVO}_4$  composites showed fasted and complete removal of dyes within 120 min. Enhanced performance of composites was credited to the smooth electron–hole

segregation and transfer, resulting in greater number of  $\bullet\text{OH}$  and  $\bullet\text{O}_2^-$  radicals for degradation reaction. Likewise, Ranjith et al. [22] synthesized the  $\text{rGO-TiO}_2/\text{Co}_3\text{O}_4$  using coprecipitation method for methylene blue degradation. The composites exhibited remarkable degradation efficiency owing to the strong integration of semiconductors over the surface reduced graphene oxide sheets. Photocatalytic performance of composite not only depend on the rGO but also optical properties of coupled semiconductor. Further, compatibility of semiconductor is important for charge generation and transfer mechanism which ultimately affects the light absorption, charge separation and degradation of dyes. Low bandgap energy metal ferrite like silver ferrite with bandgap of 1.9 eV corresponding to 620 nm wavelength, could be useful for ternary  $\text{rGO/TiO}_2$  composites [16]. The addition of low-bandgap semiconductors such as silver ferrite ( $\text{AgFeO}_2$ ) could also enhance efficiency of the  $\text{TiO}_2/\text{rGO}$  photocatalyst. The valance and conduction band energy of  $\text{AgFeO}_2$  is in the range of 1.32 eV to  $-0.5$  eV, respectively [16,23]. Due to low bandgap, heterojunction of  $\text{TiO}_2/\text{rGO}$  with  $\text{AgFeO}_2$  gives better photocatalytic efficiency in the wastewater treatment process. However, silver ferrite is unstable without any supporting material due to interstitial recombination of electron/hole which causes disintegration of silver (Ag) metal [17,18]. On the other hand, the  $\text{AgFeO}_2$  shows excellent stability when coupled with composite photocatalysts [18]. The impact of  $\text{AgFeO}_2$  addition to a photocatalyst was firstly investigated by Yin et al. [19]. It was found that  $\text{AgFeO}_2$  acted as a photocatalyst for methyl orange (MO) degradation and emitted a visible light for 150 min of irradiation. The experiment took several hours to produce significant novel results of photodegradation. The electrochemical influence of  $\text{AgFeO}_2$  on maghemite ( $\gamma\text{-Fe}_2\text{O}_3$ ) has been reported by Durham et al. [24]. It was found that fabricating electrodes in the presence of more than two composite materials enhance the energy density and efficiency of the modern batteries. However, the study based on employing  $\text{AgFeO}_2/\text{rGO/TiO}_2$  nanocomposites for photocatalytic degradation of MB in wastewater is scarce in the literature. In the nanocomposite structure, the reduced graphene oxide acts as an electron mediator and electrons transport from the semiconductor to  $\text{TiO}_2$  [19,22–26].

In this study, a ternary composite of  $\text{AgFeO}_2/\text{rGO/TiO}_2$  was investigated for MB decolorization under visible light irradiations. The  $\text{AgFeO}_2$  particles were deposited over graphene oxide followed by coupling with  $\text{TiO}_2$  using deposition method followed by reflux for 4 h at  $80^\circ\text{C}$ . The synthesized photocatalyst was characterized by using XRD, Raman and PL spectroscopy and FTIR. The performance of the  $\text{AgFeO}_2/\text{rGO/TiO}_2$  was evaluated for MB decolorization in wastewater followed by activity measurement through UV-vis spectroscopy.

## 2. Materials and Methods

### 2.1. Chemicals and Materials

The chemicals required for the preparation of  $\text{AgFeO}_2/\text{rGO/TiO}_2$  nanocomposite are graphite nano powder ( $\leq 20\text{ }\mu\text{m}$ , 99.90% Sigma Aldrich), potassium permanganate ( $\geq 99\%$ , R&M chemicals), hydrogen peroxide  $\text{H}_2\text{O}_2$  (30%, Merck), absolute ethanol  $\text{C}_2\text{H}_5\text{OH}$  (99.99% Merck), sulphuric acid (98, R&M chemicals), phosphoric acid (85%, R&M chemicals), silver nitrate (99%, Merck), iron nitrate  $\text{Fe}(\text{NO}_3)_3 \cdot 9\text{H}_2\text{O}$  (Merck), sodium hydroxide (pellets, R&M chemicals), titanium dioxide ( $\leq 21\text{ nm}$ , Anatase, 99.5%, Sigma Aldrich), methyl blue (MB).

### 2.2. Preparation of Graphene Oxide

The graphene oxide (GO) was synthesized by conventional methodology. In brief, the graphite powder (3 g) was added into 400 ml of mixed acid ( $\text{H}_2\text{SO}_4/\text{H}_3\text{PO}_4$ : 9/1) followed by gradual addition of 18 g  $\text{KMnO}_4$  under mechanical stirring. The whole reaction was taken place in an ice bath. After the addition of  $\text{KMnO}_4$ , the suspension was put in an oil bath at  $50^\circ\text{C}$  for 24 h with continuous mechanical stirring at 300 rpm. Then, 400 ml of deionized water (ice form) was added into the mixture in the at ambient temperature and 5 ml of  $\text{H}_2\text{O}_2$  was added which turned the suspension yellow. Finally, washing was done using 0.1 M HCl aqueous solution and absolute ethanol. After that, washing was

continued using deionized water until the pH of the solution reached 6. Graphite oxide was recovered by centrifugation and dried at 40 °C overnight. The obtained graphite oxide was dispersed into water and the mixture was ultrasonicated for half an hour to get graphene oxide nanosheets.

### 2.3. Preparation of $\text{AgFeO}_2/\text{rGO}/\text{TiO}_2$ Nanocomposite

The  $\text{AgFeO}_2/\text{rGO}/\text{TiO}_2$  ternary composite was synthesized using simple deposition and reflux technique.  $\text{AgNO}_3$  was dissolved in ethanol and mixed with the  $\text{Fe}(\text{NO}_3)_3$  solution at 27 °C and stirred for 2 h. The solution pH was maintained at 11–12 by adding NaOH. Similarly, a particular amount (4.0 mg) of GO was dispersed into ethanol and mixture was combined with  $\text{AgNO}_3/\text{Fe}(\text{NO}_3)_3$  suspension and stirred for 2 h. A separate suspension of  $\text{TiO}_2$  was prepared in ethanol. The obtained mixture of  $\text{Fe}(\text{NO}_3)_3/\text{AgNO}_3/\text{GO}$  was mixed with  $\text{TiO}_2$  which was dispersed earlier in the solution of ethanol. The suspension was transferred into the reflux assembly comprising of a flat-bottom vessel and condenser. Reflux was done for 3 h at 78 °C with constant stirring. After reflux, suspension was filtered and dried for 16 hours at 80 °C. The obtained composite was further calcined at 300 °C for 2 h to improve the crystallinity of final photocatalyst. In addition to this, the composition of  $\text{AgFeO}_2$  was varied from 2.5 to 5 wt.% to explore the influence of metal composition. Likewise,  $\text{AgFeO}_2/\text{TiO}_2$  was prepared through same methodology except the addition of GO.

### 2.4. Materials Characterizations

The photocatalyst was characterized using various characterization techniques. The crystalline structure of photocatalysts was studied using an X-ray diffractometer model PANalytical X'pert3 powder, (Malvern WR14 1XZ, U.K) with 5° to 90° range of diffraction angle with Cu  $\alpha$  radiations (40 kV and 30 mA) at 0.07878° scanning rate. Raman spectra were obtained employing Raman microscope with model (InVia Raman Microscope by RENISHAW UK). The laser excitation of the Raman microscope set at 514 nm in the 100–3000  $\text{cm}^{-1}$  range was used to record the spectra for Raman and PL. Fourier transform infrared spectroscopy with model SHIMADZU 8400S spectrometer, (SHIMADZU Corporation, Kyoto, Japan) was used to study the functional groups present on the photocatalysts surface with 400–4000  $\text{cm}^{-1}$  wavelengths. The sample and KBr powder were mixed in a mortar and pestle and pressed by hand to form pellet. The obtained pellet was placed in transmission holder and spectra were scanned.

### 2.5. Photocatalytic Performance Evaluation

The photocatalytic efficiency of the  $\text{AgFeO}_2/\text{rGO}/\text{TiO}_2$  was investigated for the decolorization of MB. The photocatalyst (0.01 g) of was added to 100 mL of a 10 ppm MB solution (initial and varied from 10–50 ppm), and the photocatalytic decolorization of MB was investigated in a glass reactor as shown in Figure S1. The MB solution having photocatalyst was stirred for 30 min in the dark environment to achieve adsorption–desorption equilibrium. The 1000W Xenon lamp was used as a source of light irradiations and it was hanged 15 cm above the beaker in photoreactor. However, no optical filter was employed to cut the particular wavelength of light. All the experiments were performed in the same conditions. An aliquot of MB solution (3 mL) was taken after a regular interval of 10 min during the reaction and decolorization of MB was observed using UV-visible spectrometer model UV–1602, Biotechnology Medical Services. The MB absorption spectra was analyzed after regular intervals of time.

The photocatalytic decolorization was evaluated by plotting relative concentration ( $C/C_0$ , where  $C_0$  is initial MB dye concentration and  $C$  is the MB dye concentration at certain time) of MB dye degraded with respect to degradation time (min). The rate constant,  $k$ , was calculated by considering the dye degradation reaction as pseudo first order reaction and using equation,  $\ln(C/C_0) = kt$  [25].

### 3. Results

#### 3.1. XRD Analysis

The crystallinity in the structure is an important parameter to study the optical and electrical characteristics of the nanocomposite. XRD analysis of commercial  $\text{TiO}_2$ , GO, 2.5 wt.%  $\text{AgFeO}_2/\text{rGO}/\text{TiO}_2$  and 5 wt.%  $\text{AgFeO}_2/\text{rGO}/\text{TiO}_2$  is shown in Figure 1. The GO demonstrated prominent peak at  $9.57^\circ$  corresponding to the 001 crystal plane [26]. The  $\text{TiO}_2$  showed the peaks at  $25.49^\circ$ ,  $38.64^\circ$ ,  $48.35^\circ$ ,  $54.23^\circ$ ,  $55.33^\circ$  and  $63.21^\circ$  correlate with (101), (004), (200), (105), (211), (204), and (116) crystal planes. The diffraction peaks at  $2\theta = 25.49^\circ$  explicate the anatase phase which is observed by the standard JCPDS card no. 21-1272. There was no diffraction peak at  $2\theta = 26.44^\circ$  corresponding to the rutile phase, indicating that there was only anatase  $\text{TiO}_2$ . The  $\text{AgFeO}_2/\text{rGO}/\text{TiO}_2$  composites exhibited one new peak at  $30.87^\circ$  corresponding to (102) crystal plane, which indicates the formation of  $\text{AgFeO}_2$  [27]. There were no peaks of graphene or graphene oxide due to low percentage, uniform dispersion and shielding effect of strong peak of  $\text{TiO}_2$  at  $25.49^\circ$  [28].

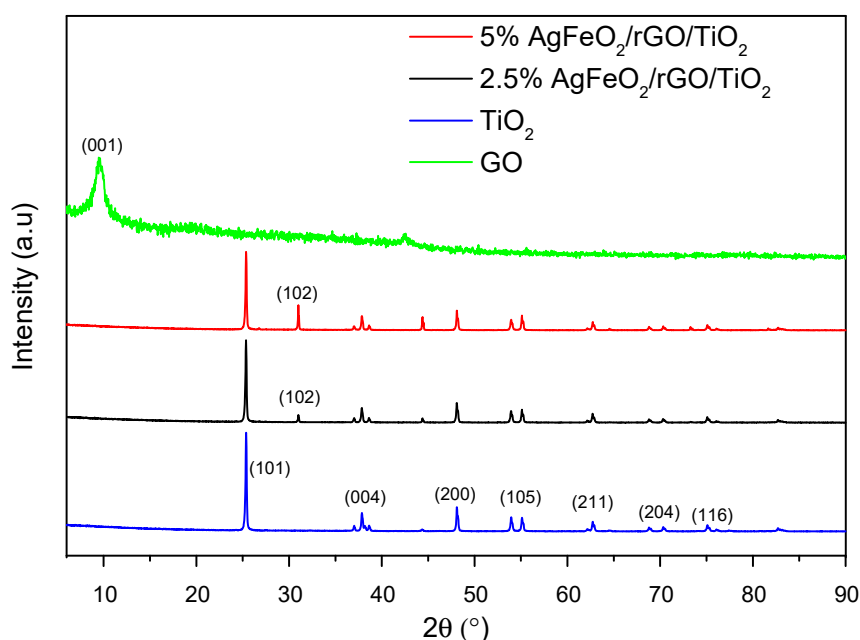


**Figure 1.** XRD pattern of Commercial Titanium dioxide ( $\text{TiO}_2$ ), graphene oxide (GO), Ternary composite photocatalyst (2.5%  $\text{AgFeO}_2/\text{rGO}/\text{TiO}_2$ ) and 5%  $\text{AgFeO}_2/\text{rGO}/\text{TiO}_2$ .

#### 3.2. FTIR Analysis

The preparation of  $\text{AgFeO}_2/\text{rGO}/\text{TiO}_2$  proceeds from the rGO bonding with  $\text{AgFeO}_2$  and with  $\text{TiO}_2$ . When rGO gets mixed with  $\text{AgFeO}_2$  and  $\text{TiO}_2$ , a chemical change occurs by the formation of new bonds which were analyzed by FTIR. The functional groups in the nanocomposite were observed with the help of FTIR (SHIMADZU 8400S) in the wavenumber range  $450\text{--}4000\text{ cm}^{-1}$ . Figure 2 shows the FTIR spectra for  $\text{TiO}_2$ , GO, and  $\text{AgFeO}_2/\text{rGO}/\text{TiO}_2$  nanocomposite. Spectra of GO shows several of oxygen functional groups and C=C bonding. The peaks at  $3446\text{ cm}^{-1}$  was ascribed to OH group. Peak at  $1638\text{ cm}^{-1}$  demonstrated the skeletal vibration of pristine graphene (C=C) structure. The small peaks at  $1420$  and  $1102\text{ cm}^{-1}$  reflected the C–O and C–O–C bonding. In addition, spectra of  $\text{TiO}_2$  showed peaks at  $3422$  and  $1622\text{ cm}^{-1}$ , showing the OH groups, whereas the peak at  $682\text{ cm}^{-1}$  reflects the Ti–O–Ti bonding. Further, spectra of  $\text{AgFeO}_2/\text{rGO}/\text{TiO}_2$  were almost like that of  $\text{TiO}_2$  and GO without any new bonding as metals do not produce any IR spectra. However, intensities of peaks are comparatively lower and, unlike GO, there is no peak at  $1420$  and  $1102\text{ cm}^{-1}$ , which shows the reduction of GO into rGO during the synthesis of  $\text{AgFeO}_2/\text{rGO}/\text{TiO}_2$ .



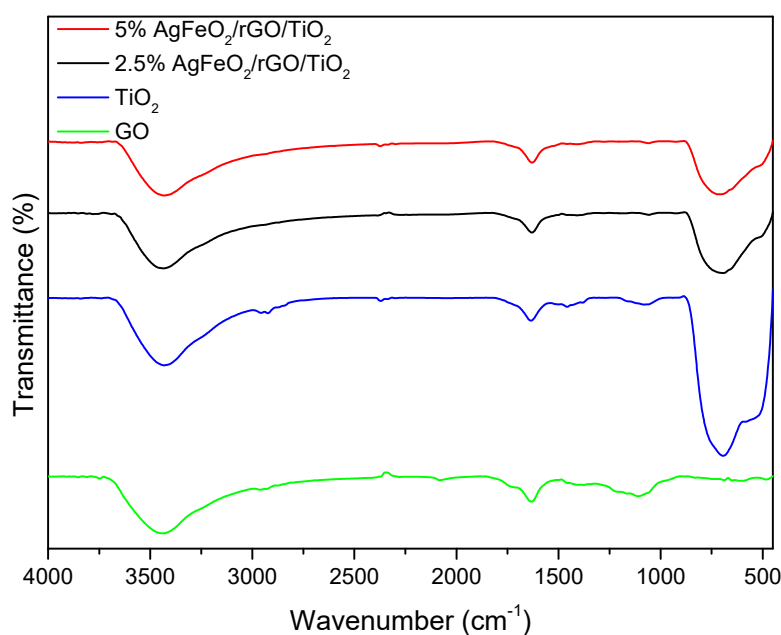


**Figure 2.** FTIR spectra of GO, Commercial  $\text{TiO}_2$ , 2.5%  $\text{AgFeO}_2/\text{rGO}/\text{TiO}_2$  and 5%  $\text{AgFeO}_2/\text{rGO}/\text{TiO}_2$ .

### 3.3. Raman Analysis

Raman spectra were recorded to analyze the chemical changes during the synthesis process. Figure 3a demonstrates the Raman spectra of  $\text{TiO}_2$ , 2.5% and 5%  $\text{AgFeO}_2/\text{rGO}/\text{TiO}_2$  measured using Laser of 514 nm. Figure 3b displays the magnified view of D and G bands for corresponding samples, i.e.,  $\text{TiO}_2$ , 2.5%  $\text{AgFeO}_2/\text{rGO}/\text{TiO}_2$  and 5%  $\text{AgFeO}_2/\text{rGO}/\text{TiO}_2$ . The D and G bands in the spectra demonstrated disorders and the in-plane  $\text{sp}^2$  behavior of graphene, respectively. The defects in the graphene structure, especially  $\text{sp}^3$  hybridized defects due to the presence of oxygen functional groups, were studied. The intensity of D band was slightly lower which indicated the disorder in the graphene  $\text{sp}^2$  due to the presence of oxygen functional groups. Estimated  $I_D/I_G$  ratio of 2.5% and 5%  $\text{AgFeO}_2/\text{rGO}/\text{TiO}_2$  were 0.88 and 0.89, respectively. The  $I_D/I_G$  showed the reduction of GO to form rGO as well as  $\text{sp}^3$  hybridized defects. Although, defects suppressed the electrical properties of graphene-based nanO-Composites, but they helped in carrying out interaction of species on photocatalyst surface. The  $\text{sp}^3$  defects due to the presence of oxygen moieties gave rise to the strong bonding between  $\text{TiO}_2$ ,  $\text{AgFeO}_2$ , and graphene sheets.

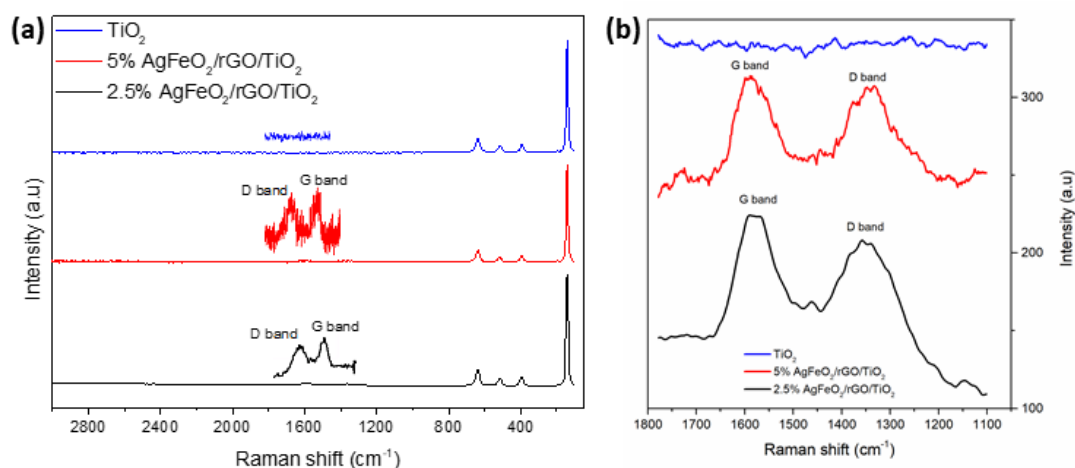


**Figure 3.** (a) Raman spectra of  $\text{TiO}_2$ , 2.5% and 5%  $\text{AgFeO}_2/\text{rGO}/\text{TiO}_2$ . (b) Magnified view of D and G bands for respective samples.

### 3.4. PL Spectroscopy

The effective charge carrier trapping, recombination, and separation were analyzed by PL spectroscopy as shown in Figure 4.  $\text{TiO}_2$  having wide band gap exhibited a high intensity of charge recombination as compared to the heterojunction photocatalyst  $\text{AgFeO}_2/\text{rGO}/\text{TiO}_2$ . This showed the electron mediator role of graphene and Z-scheme assembly of  $\text{AgFeO}_2/\text{rGO}/\text{TiO}_2$  composites. The suppressed charge recombination of  $\text{AgFeO}_2/\text{rGO}/\text{TiO}_2$  was due to formation of bridging layer of graphene which act as an electron mediator between  $\text{AgFeO}_2$  and  $\text{TiO}_2$ . This helped in effective transportation of the photogenerated electrons.

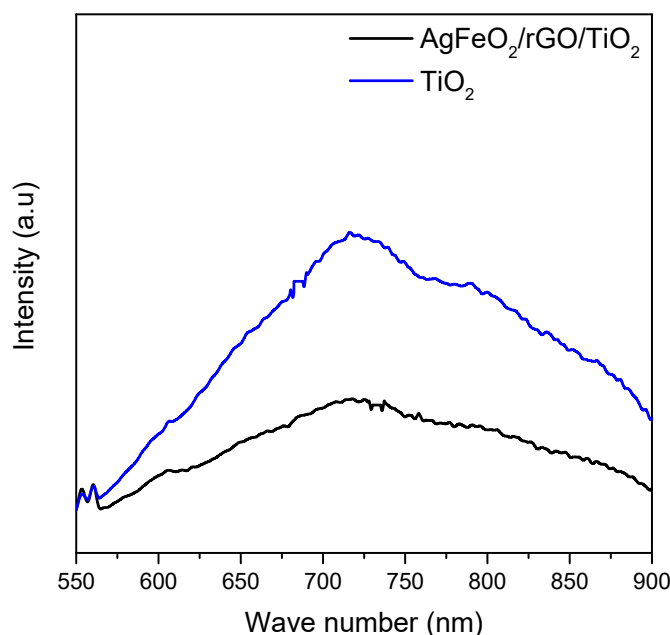
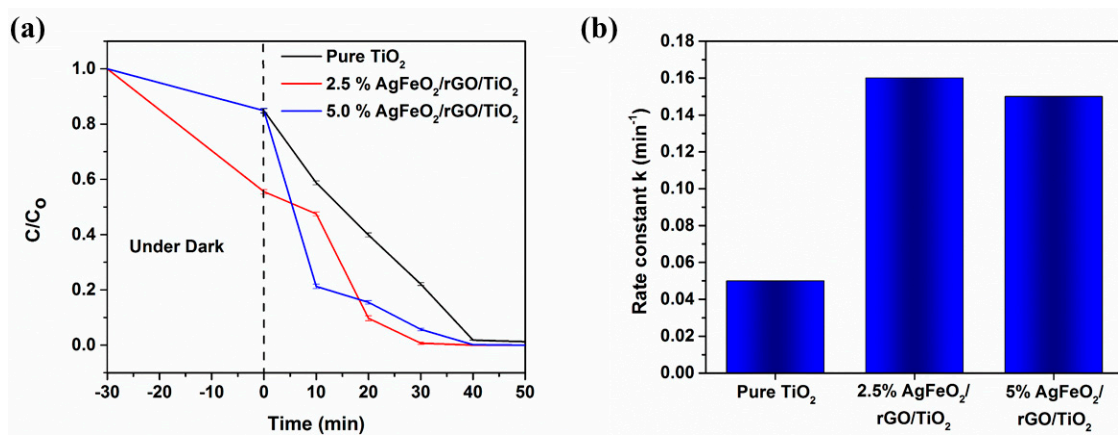


Figure 4. PL spectra of  $\text{TiO}_2$  and 2.5%  $\text{AgFeO}_2/\text{rGO}/\text{TiO}_2$ .

### 3.5. Photocatalytic Activity Test

The efficiency of photocatalysts was evaluated for MB dye decolorization with different process parameters. Figure 5a shows the plot of relative concentration ( $C/C_0$ , where  $C_0$  is initial MB dye concentration and  $C$  is the MB dye concentration) and decolorization time of MB dye employing  $\text{TiO}_2$ , 2.5% and 5%  $\text{AgFeO}_2/\text{rGO}/\text{TiO}_2$  composite samples. Dark time in the graph shows the removal of dyes due to adsorption. Interestingly, 2.5%  $\text{AgFeO}_2/\text{rGO}/\text{TiO}_2$  showed higher adsorption than 5%  $\text{AgFeO}_2/\text{rGO}/\text{TiO}_2$  and  $\text{TiO}_2$ . This could be due to the fact that increase in loading of lower surface area ferrite may reduce the overall surface area and adsorption of dyes. Therefore, 2.5%  $\text{AgFeO}_2$  gives higher dark time removal than 5%  $\text{AgFeO}_2$ . Further, the 2.5%  $\text{AgFeO}_2/\text{rGO}/\text{TiO}_2$  exhibited efficient decolorization as compared to pure  $\text{TiO}_2$  and 5%  $\text{AgFeO}_2/\text{rGO}/\text{TiO}_2$ . The higher performance of the photocatalyst could be the result of compatible loading of semiconductors as photogenerated electron-hole pairs need to be transported to  $\text{TiO}_2$  through graphene layer which is only 0.4%. However, higher rGO leads to problem of shielding effect resulting in lowering of photocatalytic activity. It can be observed that 5%  $\text{AgFeO}_2/\text{rGO}/\text{TiO}_2$  exhibited higher decolorization rate at first interval compared to 2.5%. This might have been a higher amount of photogenerated charge owing to a greater amount of ferrite loading. Nevertheless, activity was decreased in the second interval, which shows a higher charge recombination could have been started due to incompatibility ratio. On the other hand, 2.5%  $\text{AgFeO}_2/\text{rGO}/\text{TiO}_2$  showed gradual decolorization rate and also higher rate constant. Moreover, the rate constant (Figure 5b) calculated for the 2.5%  $\text{AgFeO}_2/\text{rGO}/\text{TiO}_2$  is found to be  $0.16 \text{ min}^{-1}$  which is around 3.2 times greater than those of  $\text{TiO}_2$  ( $0.05 \text{ min}^{-1}$ ). Such an efficient performance by 2.5%  $\text{AgFeO}_2/\text{rGO}/\text{TiO}_2$  can be attributed to the improved charge separation

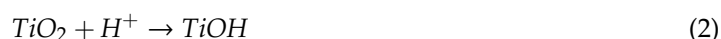
across the silver ferrite and titanium dioxide, along with suitable compositing of AgFeO<sub>2</sub> and rGO with TiO<sub>2</sub>. Additionally, the optical response exhibited by PL spectra of 2.5% AgFeO<sub>2</sub>/rGO/TiO<sub>2</sub> composite was far better due to lower bandgap of silver ferrite which enabled it to generate more charge carriers and subsequently enhanced decolorization of MB. The MB dye decolorization curves at neutral conditions for TiO<sub>2</sub>, 2.5% AgFeO<sub>2</sub>/rGO/TiO<sub>2</sub> and 5% AgFeO<sub>2</sub>/rGO/TiO<sub>2</sub> samples are shown in Figure S2. Activity of composite photocatalysts was remarkably higher than TiO<sub>2</sub>; therefore, the rest of process parameters were only tested for 2.5% and 5% AgFeO<sub>2</sub>/rGO/TiO<sub>2</sub>.



**Figure 5.** (a) Photocatalytic decolorization of MB dye solution, and (b) rate constants measured for commercial TiO<sub>2</sub>, 2.5% and 5% AgFeO<sub>2</sub>/rGO/TiO<sub>2</sub> samples.

#### Effect of Parameters

Neutral, acidic and basic pH of MB solution (50 ppm) were used in this study for photocatalytic decolorization of MB using AgFeO<sub>2</sub>/rGO/TiO<sub>2</sub> composites. The photocatalyst dosage was 0.04 g/100 mL whereas pH was adjusted to 5, 7 and 9, respectively. TiO<sub>2</sub> can be protonated or deprotonated in acidic and basic solution as depicted by Equations (1) and (2) shown below:



The photocatalytic decolorization of MB dye employing 2.5% AgFeO<sub>2</sub>/rGO/TiO<sub>2</sub> samples, in terms of relative concentration with time are shown in Figure 6a, whereas the respective rate constants calculated are shown in Figure 6b. The peculiar absorption peaks for the MB Dye degradation for respective sample are presented in Figure S3. The 2.5% AgFeO<sub>2</sub>/rGO/TiO<sub>2</sub> composite exhibited the higher performance in neutral solution than the acidic and basic solution as shown in Figure 6a. The 50 ppm solution of MB was completely degraded at 30 min in neutral media while it took 40 and 50 min to fully degrade in acidic and basic solution as shown in Table 1. The rate constant *k* for in neutral solution is found 0.09 min<sup>-1</sup> which is 2 and 2.3 times greater than the rate constants found for acidic (0.08 min<sup>-1</sup>) and basic medium (0.07 min<sup>-1</sup>), respectively.

**Table 1.** Decolorization time for MB at various pH of Dye Medium.

pH of MB Solution	Decolorization Time for 2.5% AgFeO <sub>2</sub> / rGO/TiO <sub>2</sub>	Decolorization Time for 5% AgFeO <sub>2</sub> / rGO/TiO <sub>2</sub>
Neutral (pH 7)	30 min	35 min
Acidic (pH 5)	40 min	70 min
Basic (pH 9)	50 min	50 min



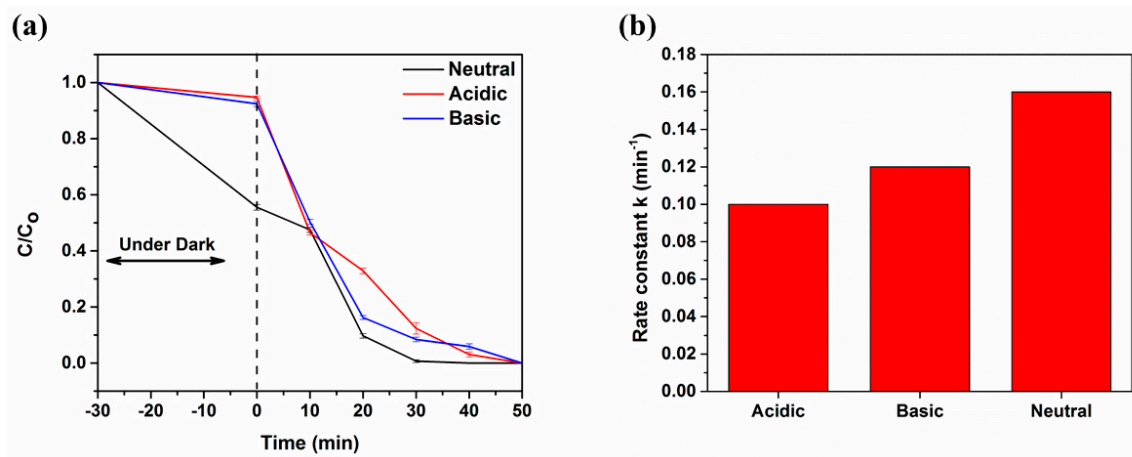


**Figure 6.** Effect of pH on MB dye decolorization for 2.5%  $\text{AgFeO}_2/\text{rGO}/\text{TiO}_2$  sample: (a) Relative concentration of MB dye decolorization with time and (b) rate constants calculated.

In acidic solution, the  $\text{TiO}_2$  surface gets positive charge [29] and in basic medium it gets negative charge. The electrostatic attraction between positive charged surface of  $\text{TiO}_2$  and MB molecules reduces the solubility of MB and enhances the absorption of light. At low pH,  $\text{TiO}_2$  shows higher oxidizing activity but the reaction rate decreases in the excess of  $\text{H}^+$  ions. The MB Dye decolorization curves for 2.5%  $\text{AgFeO}_2/\text{rGO}/\text{TiO}_2$  in neutral, acidic and basic medium are presented in in Figure S4.

Similarly, photocatalytic decolorization results of MB dye for 5%  $\text{AgFeO}_2/\text{rGO}/\text{TiO}_2$  in neutral, acidic and basic medium are shown Figure 7. Figure 7a shows the relative concentration of the MB dye degrading with time, whereas Figure 7b shows the rate constants for the various mediums. It can be observed that MB dye completely disappears after 35, 50 and 70 min for neutral, basic and acidic solutions, respectively. Herein, also the rate constants in neutral condition ( $0.09 \text{ min}^{-1}$ ) is found to be higher than those of acidic ( $0.03 \text{ min}^{-1}$ ) and basic conditions ( $0.07 \text{ min}^{-1}$ ), respectively. The MB Dye decolorization curves for 5%  $\text{AgFeO}_2/\text{rGO}/\text{TiO}_2$  in neutral, acidic and basic medium are presented in in Figure S4.

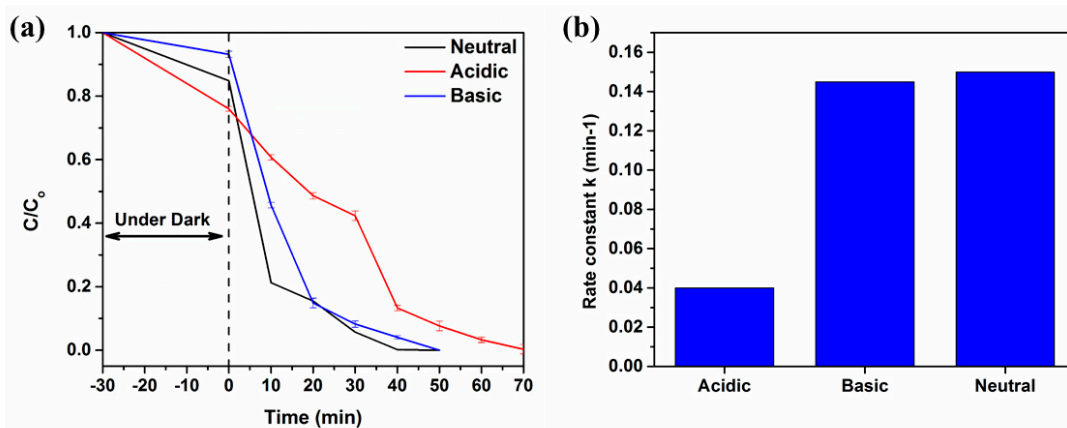


**Figure 7.** Effect of pH on MB dye decolorization for 5%  $\text{AgFeO}_2/\text{rGO}/\text{TiO}_2$  sample: (a) Relative concentration of MB dye decolorization with time and (b) rate constants calculated.

Decolorization trends are similar that of 2.5%  $\text{AgFeO}_2/\text{rGO}/\text{TiO}_2$ , i.e., neutral > acidic > basic. However, the rate of MB decolorization is faster in the 2.5%  $\text{AgFeO}_2/\text{rGO}/\text{TiO}_2$  as compared to 5%  $\text{AgFeO}_2/\text{rGO}/\text{TiO}_2$  sample. The decolorization of MB with 2.5%  $\text{AgFeO}_2/\text{rGO}/\text{TiO}_2$  and 5%  $\text{AgFeO}_2/\text{rGO}/\text{TiO}_2$  at different values of pH is shown in the below Table 1.

In addition, photocatalytic performance of photocatalysts was further investigated at different concentrations of MB solution (10, 20, 30, 40, and 50 ppm). The amount of catalyst was 0.04 g/100 mL

of solution and pH was maintained at 7. The photocatalytic decolorization of different concentration of MB solution using 2.5%  $\text{AgFeO}_2/\text{rGO}/\text{TiO}_2$  are shown in Figure 8a–e. It shows that photocatalytic process could be activated for higher concentration of dye but the decolorization rate was reduced. Figure 8 shows the wavelength-absorbance graphs concerning the decolorization of MB solutions (10 to 50 mg/L). It shows that decolorization time dye depends on concentration of the dye. The 10 ppm MB solution was fully degraded in 10 min, whereas the 50 ppm solution was completely degraded in 30 min. Thus, decolorization time was proportional to the concentration of dye.

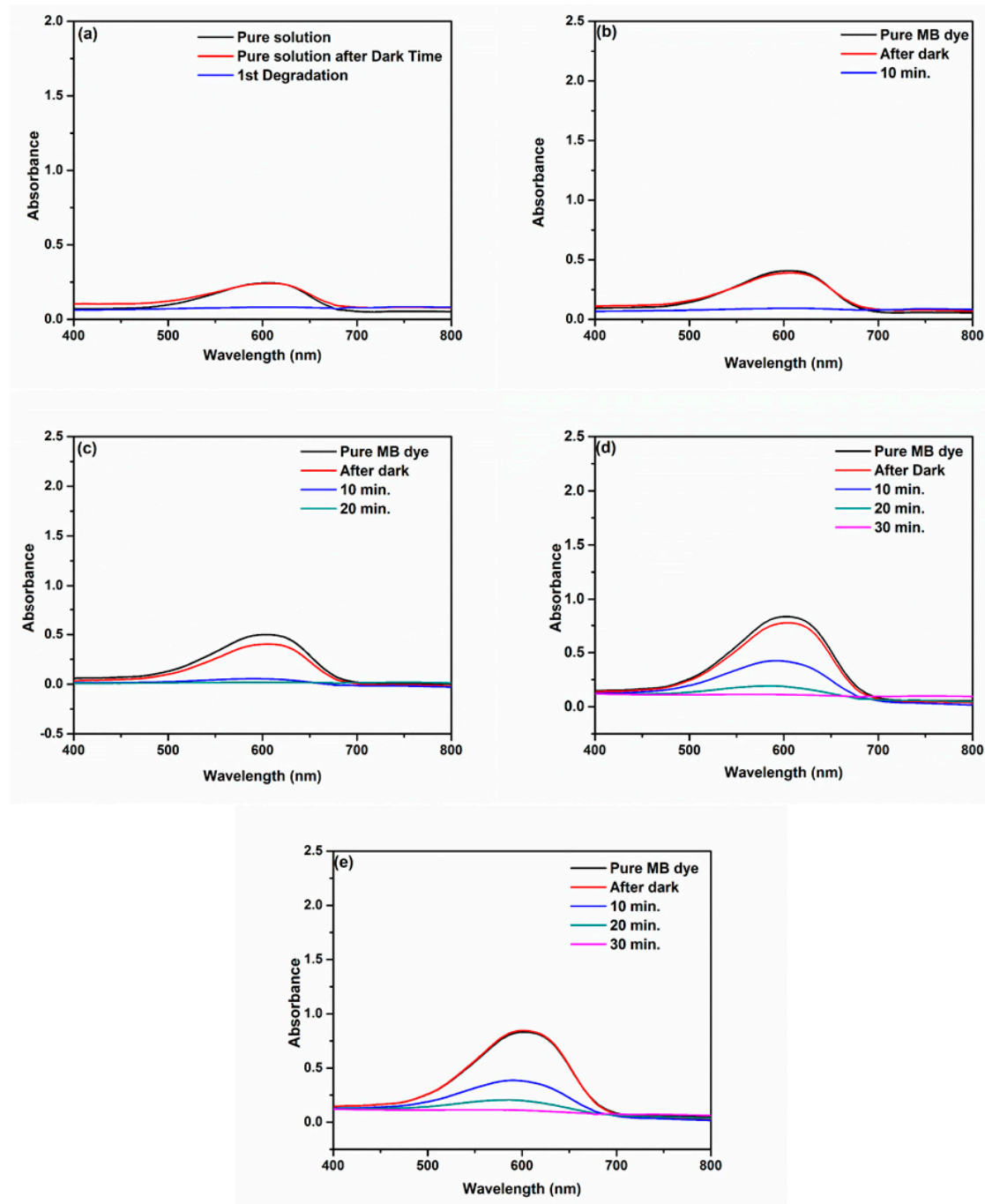


**Figure 8.** MB dye decolorization by 2.5%  $\text{AgFeO}_2/\text{rGO}/\text{TiO}_2$  photocatalyst for various concentrations: (a) 10, (b) 20, (c) 30, (d) 40, and (e) 50 ppm MB dye solution.

Similarly, Figure 9a–e shows the wavelength-absorbance graphs concerning the decolorization of MB solutions (10 to 50 mg/L) for 5%  $\text{AgFeO}_2/\text{rGO}/\text{TiO}_2$  photocatalyst. The complete decolorization

occurs in 35 min for a 50 ppm of MB solution (neutral pH). The decolorization time decreases by decreasing the concentration of dye, as shown in Table 2.

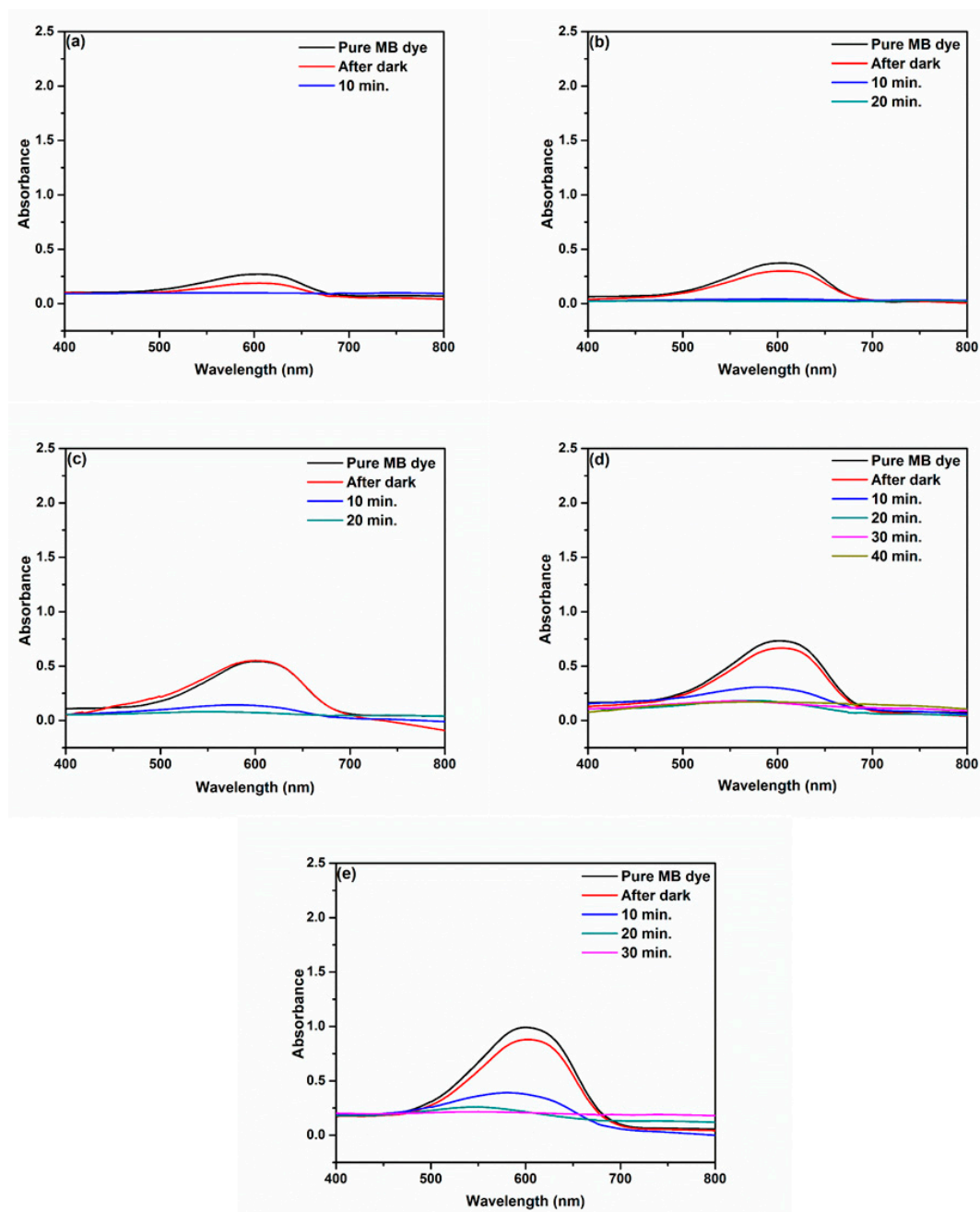


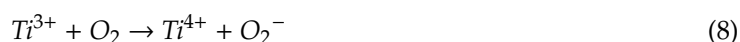
**Figure 9.** MB dye decolorization by 5% AgFeO<sub>2</sub>/rGO/TiO<sub>2</sub> photocatalyst for various concentrations: (a) 10, (b) 20, (c) 30, (d) 40, and (e) 50 ppm MB dye solution.

**Table 2.** Decolorization time for different MB Dye with various concentrations.

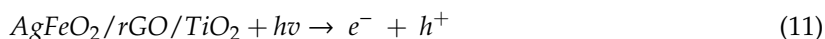
Concentration of Dye	Decolorization Time for 2.5% AgFeO <sub>2</sub> /rGO/TiO <sub>2</sub>	Decolorization Time for 5% AgFeO <sub>2</sub> /rGO/TiO <sub>2</sub>
10 ppm	8 min	10 min
20 ppm	12 min	14 min
30 ppm	18 min	20 min
40 ppm	23 min	27 min
50 ppm	30 min	35 min

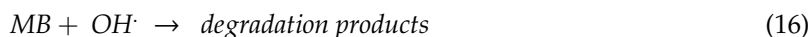
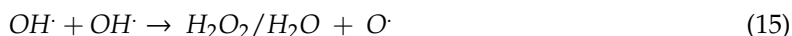
### 3.6. Mechanism of Photocatalytic Activity

Different transition metals have been used as dopants to modify the electron/hole recombination rate and bandgap energy of TiO<sub>2</sub> [21]. Meanwhile, the interaction of 3d orbital of TiO<sub>2</sub> and d orbital of the metal dopant generates intra-band gap states, which subsequently red shift towards longer wavelengths in light absorption [22,30–32]. Ferrum in Fe<sup>3+</sup> state has a very similar ionic radius to Ti<sup>4+</sup> and can substitute for Ti<sup>4+</sup> in the TiO<sub>2</sub> crystal lattice [23]. Fe<sup>3+</sup> reduces the electron/hole recombination rate significantly since it can trap electrons and holes. More importantly, the occupied states of Ti<sup>4+</sup>/Fe<sup>3+</sup> are positioned 0.5–0.8 eV above the valence band and 0.7 eV is the unoccupied states are positioned below the conduction band. This suggests that the electron/hole separation using Fe<sup>3+</sup> can occur effectively resulting in a higher lifetime of the charge carriers [33]. Despite this, Fe<sup>3+</sup> are more stable than Fe<sup>2+</sup> and Fe<sup>4+</sup>; relying on the crystal field theory by gaining or losing an electron would eventually return to the Fe<sup>3+</sup> state. Therefore, the electron and hole will be released enabling it to move to the plane of the catalyst [34]. The mechanism of electron/hole trapping and they are passing through the plane to create free radicals are described as follows Equations (3)–(10) [35].



When visible light is irradiated on the surface of the AgFeO<sub>2</sub>/rGO/TiO<sub>2</sub> present in the MB solution in the photoreactor, photogenerated electron–hole pairs are produced Equation (11). The visible light irradiated on water also produce reactive species such as H<sub>2</sub>O and OH as given in Equations (12) and (13). The photogenerated h<sup>+</sup> also participate in the reaction to produce different active species such as OH<sup>•</sup> Equation (14). The hydroxyl radicals formed are highly reactive and react with each other to form H<sub>2</sub>O<sub>2</sub> Equation (15). The OH has high oxidation potential (2.8 eV) and is non-specific in nature; therefore, it reacts with MB molecules immediately and decomposes them into smaller and harmless products such as CO<sub>2</sub> and H<sub>2</sub>O (16) [36,37].





#### 4. Conclusions

The AgFeO<sub>2</sub>/rGO/TiO<sub>2</sub> composites are successfully prepared into two-step processes: (i) deposition; (ii) reflux method. The prepared nanocomposites were characterized by using different characterization techniques like XRD, FTIR, RAMAN and photoluminescence spectroscopy. The results showed that the properties of nanocomposite were significantly improved leading to higher efficiency. The composition of AgFeO<sub>2</sub> was varied from 2.5 to 5 wt.% to analyze the contribution of metal in the nanocomposite. The activity of 2.5 wt.% AgFeO<sub>2</sub>/rGO/TiO<sub>2</sub> was higher than the 5 wt.% AgFeO<sub>2</sub>/rGO/TiO<sub>2</sub> due to the compatibility between charge generation active metal ferrite and consumption over support and successful utilization of electron and hole in dyes decolorization reaction. Parametric study showed that dyes decolorization was fast in neutral solution as compared to acidic and basic conditions. Further, time to degrade the dyes was increasing with increase of MB concentration and 50 ppm was completely degraded in 30 min. The photocatalytic activity of nanocomposite was attributed to the efficient electron–hole separation, reduced charge recombination, and improved optical response.

**Supplementary Materials:** The following are available online at <http://www.mdpi.com/2073-4352/10/10/923/s1>, Figure S1: Schematic of experimental setup, Figure S2: Absorption spectra for MB dye degradation under neutral conditions for (a) TiO<sub>2</sub>, (b) 2.5% AgFeO<sub>2</sub>/rGO/TiO<sub>2</sub> and (c) 5% AgFeO<sub>2</sub>/rGO/TiO<sub>2</sub>, Figure S3: Absorption spectra for MB dye degradation for 2.5% AgFeO<sub>2</sub>/rGO/TiO<sub>2</sub> under (a) neutral, (b) acidic and (c) basic conditions, Figure S4: Absorption spectra for MB dye degradation for 5% AgFeO<sub>2</sub>/rGO/TiO<sub>2</sub> under (a) neutral, (b) acidic and (c) basic conditions.

**Author Contributions:** Conceptualization, N.S. and M.Z.; Investigation A.R. and M.A.; Data curation, W.Y.K.; Visualization, M.A.; Writing—original draft preparation, A.R. and N.S.; Writing—review and editing, M.Z. and W.Y.K.; Supervision, M.H. and P.A.; Methodology; N.A., A.H. and K.A.; Funding acquisition, W.Y.K. and M.H. All authors have read and agreed to the published version of the manuscript.

**Funding:** This work was supported by the Basic Science Research Program through the National Research Foundation of Korea (NRF) grant funded by the Korea Government (Ministry of Science and ICT) (NRF-2018R1A4A1025998). This work was also partially supported by Higher Education Commission of Pakistan (HEC) under Technology Development Fund project (TDF02-011).

**Conflicts of Interest:** The authors declare no conflict of interest.

#### References

1. Denchak, M. The dirty fight over Canadian tar sands oil. *NRDC. Dec.* **2015**, *31*, 2015.
2. Ayadi, I.; Souissi, Y.; Jlassi, I.; Peixoto, F.P.; Mnif, W. Chemical Synonyms, Molecular Structure and Toxicological Risk Assessment of Synthetic Textile Dyes: A Critical Review. *J. Dev. Drugs* **2015**, *5*, 2. [\[CrossRef\]](#)
3. Rahman, R.A.; Ibrahim, H.A.; Hung, Y.-T. Liquid Radioactive Wastes Treatment: A Review. *Water* **2011**, *3*, 551–565. [\[CrossRef\]](#)
4. Rauf, M.; Ashraf, S.S. Fundamental principles and application of heterogeneous photocatalytic degradation of dyes in solution. *Chem. Eng. J.* **2009**, *151*, 10–18. [\[CrossRef\]](#)
5. Han, S.; Li, J.; Yang, K.; Lin, J. Fabrication of a β-Bi<sub>2</sub>O<sub>3</sub>/BiOI heterojunction and its efficient photocatalysis for organic dye removal. *Chin. J. Catal.* **2015**, *36*, 2119–2126. [\[CrossRef\]](#)
6. Mendez, P.; Manríquez, J.; Rodríguez, F.J.; Bustos, E.; Rodríguez, A.; Ortiz-Frade, L.; Godínez, L.A. Study of the Conductivity Mechanism of Non-Illuminated TiO<sub>2</sub> Electrodes Modified with Bipyridine- and Terpyridine-Ru(II) Complexes. *J. Electrochem. Soc.* **2013**, *160*, H836–H840. [\[CrossRef\]](#)
7. Park, N.-G.; Van De Lagemaat, J.; Frank, A.J. Comparison of Dye-Sensitized Rutile- and Anatase-Based TiO<sub>2</sub>Solar Cells. *J. Phys. Chem. B* **2000**, *104*, 8989–8994. [\[CrossRef\]](#)

8. Riegel, G.; Bolton, J.R. Photocatalytic Efficiency Variability in TiO<sub>2</sub> Particles. *J. Phys. Chem.* **1995**, *99*, 4215–4224. [\[CrossRef\]](#)
9. Chen, C.-C.; Li, X.; Ma, W.; Zhao, J.; Hidaka, H.; Serpone, N. Effect of Transition Metal Ions on the TiO<sub>2</sub>-Assisted Photodegradation of Dyes under Visible Irradiation: A Probe for the Interfacial Electron Transfer Process and Reaction Mechanism. *J. Phys. Chem. B* **2002**, *106*, 318–324. [\[CrossRef\]](#)
10. Fujishima, A.; Zhang, X.; Tryk, D. TiO<sub>2</sub> photocatalysis and related surface phenomena. *Surf. Sci. Rep.* **2008**, *63*, 515–582. [\[CrossRef\]](#)
11. Lui, G.; Liao, J.-Y.; Duan, A.; Zhang, Z.; Fowler, M.; Yu, A. Graphene-wrapped hierarchical TiO<sub>2</sub> nanoflower composites with enhanced photocatalytic performance. *J. Mater. Chem. A* **2013**, *1*, 12255. [\[CrossRef\]](#)
12. Jo, W.-K.; Kang, H.-J. Titanium dioxide–graphene oxide composites with different ratios supported by Pyrex tube for photocatalysis of toxic aromatic vapors. *Powder Technol.* **2013**, *250*, 115–121. [\[CrossRef\]](#)
13. Kerkez-Kuyumcu, Ö.; Kibar, E.; Dayıoğlu, K.; Gedik, F.; Akın, A.N.; Özkara-Aydinoğlu, Ş. A comparative study for removal of different dyes over M/TiO<sub>2</sub> (M = Cu, Ni, Co, Fe, Mn and Cr) photocatalysts under visible light irradiation. *J. Photochem. Photobiol. A Chem.* **2015**, *311*, 176–185. [\[CrossRef\]](#)
14. Asilturk, M.; Sayılkan, F.; Arpaç, E. Effect of Fe<sup>3+</sup> ion doping to TiO<sub>2</sub> on the photocatalytic degradation of Malachite Green dye under UV and vis-irradiation. *J. Photochem. Photobiol. A Chem.* **2009**, *203*, 64–71. [\[CrossRef\]](#)
15. Pastrana-Martínez, L.M.; Morales-Torres, S.; Likodimos, V.; Figueiredo, J.L.; Faria, J.L.; Falaras, P.; Silva, A.M. Advanced nanostructured photocatalysts based on reduced graphene oxide–TiO<sub>2</sub> composites for degradation of diphenhydramine pharmaceutical and methyl orange dye. *Appl. Catal. B Environ.* **2012**, *123*, 241–256. [\[CrossRef\]](#)
16. Wang, F.; Zhang, K. Reduced graphene oxide–TiO<sub>2</sub> nanocomposite with high photocatalytic activity for the degradation of rhodamine B. *J. Mol. Catal. A Chem.* **2011**, *345*, 101–107. [\[CrossRef\]](#)
17. Yin, X.; Zhang, H.; Xu, P.; Han, J.; Li, J.; He, M. Simultaneous N-doping of reduced graphene oxide and TiO<sub>2</sub> in the composite for visible light photodegradation of methylene blue with enhanced performance. *RSC Adv.* **2013**, *3*, 18474. [\[CrossRef\]](#)
18. Muthirulan, P. Fabrication And Characterization Of Efficient Hybrid Photocatalysts Based On Titania And Graphene For Acid Orange Seven Dye Degradation Under UV Irradiation. *Adv. Mater. Lett.* **2014**, *5*, 163–171. [\[CrossRef\]](#)
19. Shehzad, N.; Tahir, M.; Johari, K.; Murugesan, T.; Hussain, M. A critical review on TiO<sub>2</sub> based photocatalytic CO<sub>2</sub> reduction system: Strategies to improve efficiency. *J. CO<sub>2</sub> Util.* **2018**, *26*, 98–122. [\[CrossRef\]](#)
20. Shehzad, N.; Maafa, I.M.; Johari, K.; Hafeez, A.; Akhter, P.; Shabir, M.; Raza, A.; Anjum, H.; Hussain, M.; Tahir, M. Carbon Nanotubes Incorporated Z-Scheme Assembly of AgBr/TiO<sub>2</sub> for Photocatalytic Hydrogen Production under Visible Light Irradiations. *Nanomaterials* **2019**, *9*, 1767. [\[CrossRef\]](#)
21. Samsudin, M.F.R.; Mahmood, A.; Sufian, S. Enhanced Photocatalytic Degradation of Wastewater over RGO-TiO<sub>2</sub>/BiVO<sub>4</sub> photocatalysts Under Solar Light Irradiation. *J. Mol. Liq.* **2018**, *268*, 26–36. [\[CrossRef\]](#)
22. Ranjith, R.; Renganathan, V.; Chen, S.-M.; Selvan, N.S.; Rajam, P.S. Green synthesis of reduced graphene oxide supported TiO<sub>2</sub>/Co<sub>3</sub>O<sub>4</sub> nanocomposite for photocatalytic degradation of methylene blue and crystal violet. *Ceram. Int.* **2019**, *45*, 12926–12933. [\[CrossRef\]](#)
23. Yin, L.; Shi, Y.; Lu, L.; Fang, R.; Wan, X.-K.; Shi, H. A Novel Delafossite Structured Visible-Light Sensitive AgFeO<sub>2</sub> Photocatalyst: Preparation, Photocatalytic Properties, and Reaction Mechanism. *Catalysts* **2016**, *6*, 69. [\[CrossRef\]](#)
24. Durham, J.L.; Kirshenbaum, K.; Takeuchi, E.S.; Marschilok, A.C.; Takeuchi, K.J. In-situ Formation of a Series of AgFeO<sub>2</sub>/γ-Fe<sub>2</sub>O<sub>3</sub> Composites: Impact on Electrochemical Performance. *MRS Adv.* **2016**, *1*, 389–394. [\[CrossRef\]](#)
25. Zubair, M.; Kim, H.; Razzaq, A.; Grimes, C.A.; In, S.-I. Solar spectrum photocatalytic conversion of CO<sub>2</sub> to CH<sub>4</sub> utilizing TiO<sub>2</sub> nanotube arrays embedded with graphene quantum dots. *J. CO<sub>2</sub> Util.* **2018**, *26*, 70–79. [\[CrossRef\]](#)
26. Shehzad, N.; Johari, K.; Murugesan, T.; Tahir, M. Graphene Oxide as An Efficient Photocatalyst For Photocatalytic Reduction of CO<sub>2</sub> Into Solar Fuel. *Int. J. Automot. Mech. Eng.* **2018**, *15*, 4909–4918. [\[CrossRef\]](#)
27. Farley, K.E.; Marschilok, A.C.; Takeuchi, E.S.; Takeuchi, K.J. Synthesis and Electrochemistry of Silver Ferrite. *Electrochem. Solid-State Lett.* **2011**, *15*, A23–A27. [\[CrossRef\]](#)



28. Shehzad, N.; Tahir, M.; Johari, K.; Murugesan, T.; Hussain, M. Improved interfacial bonding of graphene-TiO<sub>2</sub> with enhanced photocatalytic reduction of CO<sub>2</sub> into solar fuel. *J. Environ. Chem. Eng.* **2018**, *6*, 6947–6957. [[CrossRef](#)]
29. Park, S.-K.; Shin, H. Effect of HCl and H<sub>2</sub>SO<sub>4</sub> treatment of TiO<sub>2</sub> powder on the photosensitized degradation of aqueous rhodamine B under visible light. *J. Nanosci. Nanotechnol.* **2014**, *14*, 8122–8128. [[CrossRef](#)] [[PubMed](#)]
30. Devi, L.G.; Kottam, N.; Murthy, B.N.; Kumar, S.G. Enhanced photocatalytic activity of transition metal ions Mn<sup>2+</sup>, Ni<sup>2+</sup> and Zn<sup>2+</sup> doped polycrystalline titania for the degradation of Aniline Blue under UV/solar light. *J. Mol. Catal. A Chem.* **2010**, *328*, 44–52. [[CrossRef](#)]
31. Kemp, T.J.; McIntyre, R.A. Transition metal-doped titanium (IV) dioxide: Characterisation and influence on photodegradation of poly (vinyl chloride). *Polym. Degrad. Stab.* **2006**, *91*, 165–194. [[CrossRef](#)]
32. Santos, R.S.; Faria, G.A.; Giles, C.; Leite, C.A.P.; Barbosa, H.D.S.; Arruda, M.A.Z.; Longo, C. Iron Insertion and Hematite Segregation on Fe-Doped TiO<sub>2</sub> Nanoparticles Obtained from Sol–Gel and Hydrothermal Methods. *ACS Appl. Mater. Interfaces* **2012**, *4*, 5555–5561. [[CrossRef](#)]
33. Shough, A.M.; Doren, D.J.; Ogunnaike, B.A. Transition Metal Substitution in ETS-10: DFT Calculations and a Simple Model for Electronic Structure Prediction. *Chem. Mater.* **2009**, *21*, 1232–1241. [[CrossRef](#)]
34. Zhou, M.; Yu, J.; Cheng, B. Effects of Fe-doping on the photocatalytic activity of mesoporous TiO<sub>2</sub> powders prepared by an ultrasonic method. *J. Hazard. Mater.* **2006**, *137*, 1838–1847. [[CrossRef](#)]
35. Rauf, M.; Meetani, M.; Hisaindee, S. An overview on the photocatalytic degradation of azo dyes in the presence of TiO<sub>2</sub> doped with selective transition metals. *Desalination* **2011**, *276*, 13–27. [[CrossRef](#)]
36. Zhang, J.; Xu, H.; Chen, H.; Anpo, M. Study on the formation of H<sub>2</sub>O<sub>2</sub> on TiO<sub>2</sub> photocatalysts and their activity for the photocatalytic degradation of X-GL dye. *Res. Chem. Intermed.* **2003**, *29*, 839–848. [[CrossRef](#)]
37. Attri, P.; Kim, Y.H.; Park, D.H.; Park, J.H.; Hong, Y.J.; Uhm, H.S.; Kim, K.-N.; Fridman, A.; Choi, E.H. Generation mechanism of hydroxyl radical species and its lifetime prediction during the plasma-initiated ultraviolet (UV) photolysis. *Sci. Rep.* **2015**, *5*, 9332. [[CrossRef](#)]



© 2020 by the authors. Licensee MDPI, Basel, Switzerland. This article is an open access article distributed under the terms and conditions of the Creative Commons Attribution (CC BY) license (<http://creativecommons.org/licenses/by/4.0/>).